THE PLANCK LOW FREQUENCY INSTRUMENT

Thermal susceptibility of the Planck-LFI receivers

L. Terenzi,[a,1] **M.J. Salmon, A. Colin,**[b] **A. Mennella,**[c] **G. Morgante,**[a] **M. Tomasi,**[c]
P. Battaglia,[d] **M. Lapolla,**[d] **M. Bersanelli,**[c] **R.C. Butler,**[a] **F. Cuttaia,**[a] **O. D'Arcangelo,**[e]
R. Davis,[f] **C. Franceschet,**[d] **S. Galeotta,**[g] **A. Gregorio,**[h,g] **N. Hughes,**[i] **P. Jukkala,**[i]
D. Kettle,[l] **M. Laaninen,**[k] **P. Leutenegger,**[d] **R. Leonardi,**[m] **N. Mandolesi,**[a] **M. Maris,**[g]
P. Meinhold,[m] **M. Miccolis,**[d] **N. Roddis,**[f] **L. Sambo,**[a] **M. Sandri,**[a] **R. Silvestri,**[d]
J. Tuovinen,[j] **L. Valenziano,**[a] **J. Varis,**[j] **F. Villa,**[a] **A. Wilkinson**[f] **and A. Zonca**[n]

[a] *INAF - IASF Bologna, via P. Gobetti 101, 40129 Bologna, Italy*

[b] *Instituto de Física de Cantabria (CSIC-UC), Av. Los Castros s/n. 39005 Santander, Spain*

[c] *Università degli Studi di Milano, Via Celoria 16, 20133 Milano, Italy*

[d] *Thales Alenia Space Italia, Sede di Milano, S.S. Padana Superiore 290, 20090, Vimodrone, Italy*

[e] *Istituto di Fisica del Plasma CNR, via Cozzi 53, 20125 Milan, Italy*

[f] *Jodrell Bank Centre for Astrophysics,*
  Alan Turing Building, The University of Manchester, Manchester, M13 9PL, U.K.

[g] *INAF Osservatorio Astronomico di Trieste, via Tiepolo 11, Trieste 34143, Italy*

[h] *University of Trieste, Department of Physics, via Valerio 2, Trieste 34127, Italy*

[i] *DA-Design Oy, Keskuskatu 29, FI-31600, Jokioinen, Finland*

[j] *MilliLab, VTT Technical Research Centre of Finland, Tietotie 3, Otaniemi, Espoo, Finland*

[k] *Ylinen Electronics Oy, Teollisuustie 9A, FIN-02700 Kauniainen, Finland*

[l] *School of Electrical and Electronic Engineering, The University of Manchester,*
  Manchester, M60 1QD, U.K.

[m] *Department of Physics, University of California, Santa Barbara, CA 93106, U.S.A.*

[n] *INAF IASF Milano, Via Bassini 15, 20133 Milano, Italy*

 E-mail: terenzi@iasfbo.inaf.it

ABSTRACT: This paper describes the impact of the Planck Low Frequency Instrument front end physical temperature fluctuations on the output signal. The origin of thermal instabilities in the instrument are discussed, and an analytical model of their propagation and impact on the receivers signal is described. The experimental test setup dedicated to evaluate these effects during the instrument ground calibration is reported together with data analysis methods. Finally, main results obtained are discussed and compared to the requirements.

KEYWORDS: Systematic effects; Space instrumentation; Microwave radiometers; Instruments for CMB observations

---

[1]Corresponding author.

Contents

1 Introduction

Planck is an ESA mission designed to map with high precision the angular distribution of the Cosmic Microwave Background (CMB). The Planck observations are expected to produce major steps forward for precision cosmology as well as for Galactic and extragalactic millimeter-wave astrophysics [9].

The Planck measurements will span over a wide range of frequencies by means of the two instruments on board: the Low Frequency Instrument (LFI, [3]) ranging from 30 to 70 GHz, and the High Frequency Instrument (HFI, [2]), from 100 to 850 GHz.

LFI is an array of 22 pseudo-correlation radiometers (two for each feed horn, [1]), whose core elements are HEMT-based low noise amplifiers located in the Front End Modules (FEMs). Radiometers are labelled as Main and Side arms for each of the Radiometer Chain Assemblies (RCAs) fed by one horn. The signal coming from the sky is compared continuously to the emission of the 4 K reference load (4K RL, [13]), consisting of small blackbodies connected to the High Frequency Instrument shield at a temperature of about 4 K.

The ambitious Planck scientific goal to finely map sky temperature differences at level of μK requires a strict control of time variations in the signal due to environmental systematic effects such as thermal or electrical instabilities.

In this paper the susceptibility of the radiometers to temperature fluctuations is studied.

The presence of active coolers, mainly the 20 K sorption cooler [6], in the satellite cryogenic chain produces temperature instabilities in different stages of the instruments.

The two sorption cooler cold ends give the reference temperature to the LFI focal plane and main frame and serve as precooling stage for the 4 K cooler of the HFI.

Fluctuations generated in the sorption cooler are thus responsible for temperature oscillations both in the LFI amplifiers, located on the focal plane, and in the 4K Reference Load, mounted on the HFI outer shield.

These temperature fluctuations produce a signal variation which mimics the observed CMB temperature anisotropies. The accurate knowledge of the impact of physical temperature fluctuations on output antenna temperature fluctuations is therefore fundamental to estimate the error induced by this systematic effect on the LFI observations.

In this paper we focus on the effect of temperature fluctuations in the instrument front end. They have been modeled and subsequently measured during two instrument ground test campaigns:

- the Radiometer Chain Assembly (RCA) level test [14], where each single radiometer chain associated to the same sky horn was tested indipendently

- the Radiometer Array Assembly (RAA) level test [5], where all the RCAs were integrated together and the whole Low Frequency Instrument was tested

The theoretical fundamentals of LFI radiometer susceptibility to thermal effects are outlined in section 2.

In section 3, we discuss in detail the susceptibility measurements, describing the experimental setup and data analysis methods and summarizing the obtained results.

Finally in section 4, the main conclusions are drawn.

2 Effect of focal plane thermal fluctuations on LFI radiometers signal

2.1 The thermal systematic effects

The active elements of the Planck LFI radiometers are located in the Front End Modules (FEMs) and Back End Modules (BEMs).

Fluctuations in the physical temperature of these modules affect the basic properties of the low noise amplifiers, such as noise temperature and gain, causing a correlated fluctuation in the output signal.

An analytical expression for the measured radiometer output, p_{out}, can be expressed as a function of the sky and reference load input signals, and of parameters which are temperature dependent, such as amplifiers' gain and noise temperature, which we indicate here generically as K_i, $p_{out} \equiv p_{out}(T_s, T_{4K}, K_i)$ (see [8] for details).

The sky signal fluctuation, δT_s, equivalent to the systematic effect induced by thermal fluctuation, δT_{phys}, can then be evaluated from:

$$\frac{\partial p}{\partial T_s} \cdot \delta T_s = \frac{\partial p}{\partial T_{phys}} \cdot \delta T_{phys} \qquad (2.1)$$

so that we can define a radiometric transfer function for physical temperature fluctuation:

$$T_f^{id} = \frac{\frac{\partial p}{\partial T_{phys}^{id}}}{\frac{\partial p}{\partial T_s}} \qquad (2.2)$$

where the index *id* identifies the different temperature stages whose fluctuations have an impact on the signal output, FEM, BEM, 4 K RL being the most relevant.

Generally the dependence of p_{out} on temperature is not explicit, but embedded in the temperature dependence of the various instrument parameters K_i, so that we have:

$$\frac{\partial p}{\partial T_{phys}} \equiv \sum_i \frac{\partial p_{out}}{\partial K_i} \cdot \frac{\partial K_i}{\partial T_{phys}} \tag{2.3}$$

Once the transfer function T_f is defined, we can characterize how temperature changes in the instrument impact on the signal by means of the relation:

$$\delta T_s = T_f \cdot \delta T_{phys} \tag{2.4}$$

As thermal instabilities mimic signal variations in a direct way, in defining the requirement levels for this kind of systematic effect, we have to treat carefully the spin synchronous fluctuations which would be undistinguishable from the sky signal.

The maximum allowable spurious signal caused by focal plane thermal fluctuations must be lower than 1 μK (0.9 μK for a generic periodic fluctuation and 0.45 μK for a spin synchronous fluctuation, [1]).

As explained in the following and finally discussed in the last section, different properties of the instrument have to be taken into account, in order to accurately control this systematic effect and verify the compliance with requirements.

2.1.1 The source of front end thermal instability: the hydrogen sorption cooler

The LFI first stage of signal amplification is located in the Focal Plane Unit (FPU) of the instrument, cooled at 20 K by the hydrogen sorption cooler [6].

The cooler consists of six compressor elements absorbing and desorbing hydrogen gas in a sequential way to create liquid in its cold ends (liquid-vapour heat exchangers, LVHXs) through a JT expansion. The temperature at the cooler cold ends fluctuates at the level of $\sim$ 400 mK peak to peak, with a spectrum dominated by two main frequencies: the compressor element cycle, typically in the range 600–1000 s, and at the period of the whole cooler, six times longer than the previous one.

In order to significantly reduce undesired fluctuations, an active temperature control stage, the Thermal Stabilization Assembly (TSA), based on a PID algorithm was inserted between the LVHX2 and the LFI main frame.

Typical sorption cooler temperature fluctuations are shown in figure 1, which displays two timestreams: the black line corresponds to the cold end temperature and the red line corresponds to the temperature downstream of the TSA, whose effect is to decrease the peak-to-peak amplitude to below 100 mK; in particular, it is effective in the lower frequencies part of the spectrum and the two main periods of the cooler are strongly reduced.

Temperature fluctuations propagate through the LFI mechanical structure and are damped by the LFI front end thermal mass, which acts as a low pass filter. This effect was first studied by means of a dedicated thermal model of the instrument and then measured during instrument level ground test (see [11] for details).
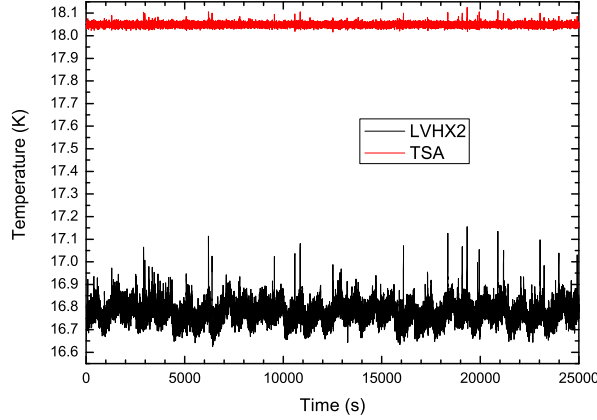
Figure 1. A typical temperature curve of the LVHX2 sorption cooler cold end (black line) during ground tests. The temperature after thermal stabilization is also shown (red line).

2.2 Transfer function between front end temperature variations and the radiometer signal

If $\delta T_{\text{phys}}^{\text{FEM}}$ is the temperature fluctuation at the level of the front-end module, then the systematic variation induced in antenna temperature output is given by:

$$\delta T_s = T_f^{\text{FEM}} \cdot \delta T_{\text{phys}}^{\text{FEM}}$$

The main contributions to the radiometer output equation coming from the instrument 20 K stage are given by the amplifiers gain and noise temperature, and the attenuation of the signal coming from the sky, the feed horns and OMT insertion losses, and from the reference load, by the reference horn loss. The properties related to the electronic active devices are known to be affected at a significant and measurable level by fluctuations of the order of a few K, while passive losses, which depend on geometrical and material properties, are considered constant in the typical temperature range where the fluctuations occurred.

Applying eq. (2.2) to the radiometer differenced output expression (reported in the appendix, eq. (A.1)), an analytical expression for the transfer function can be found as:

$$
\begin{aligned}
T_f^{\text{FEM}} = {} & \left(\frac{L_{fh-OMT}}{(G_{F1}+G_{F2})\cdot(1-r)+2\cdot\sqrt{G_{F1}\cdot G_{F2}}\cdot(1+r)} \right) \cdot \left[\left(\frac{\partial G_{F1}}{\partial T_{\text{phys}}^{\text{FEM}}} \right) \cdot \left((T_{\text{sky}}+T_{4K}+2\cdot T_{nF1})\cdot(1-r)+\sqrt{\tfrac{G_{F2}}{G_{F1}}}\cdot(1+r) \right) + \right. \\
& \left(\frac{\partial G_{F2}}{\partial T_{\text{phys}}^{\text{FEM}}} \right) \cdot \left((T_{\text{sky}}+T_{4K}+2\cdot T_{nF2})+\cdot(1-r)+\sqrt{\tfrac{G_{F1}}{G_{F2}}}\cdot(1+r) \right) + \left(\frac{\partial T_{nF1}}{\partial T_{\text{phys}}^{\text{FEM}}} \right) \cdot \left(2\cdot G_{F1}\cdot(1-r) \right) + \left(\frac{\partial T_{nF2}}{\partial T_{\text{phys}}^{\text{FEM}}} \right) \cdot \left(2\cdot G_{F2}\cdot(1-r) \right) + \\
& \left. \left(1-\frac{1}{L_{fh-OMT}} \right) \cdot \left((G_{F1}+G_{F2})\cdot(1-r)+2\cdot\sqrt{G_{F1}\cdot G_{F2}}\cdot(1+r) \right) + \left(1-\frac{1}{L_{4K}} \right) \cdot \left((G_{F1}+G_{F2})\cdot(1-r)-2\cdot\sqrt{G_{F1}\cdot G_{F2}}\cdot(1+r) \right) \right] \quad (2.5)
\end{aligned}
$$

where:

- L_i are insertion losses either for the feed horn-OMT system or for the 4K horn antenna; in our analysis we assume their values estimated from measurements at room temperature;

- r is the *gain modulation factor* used to balance the sky and reference output signals; its value is evaluated from the ratio of sky to reference channel mean voltage values;

- G_{Fi} are the front end amplifier gains, whose typical value is about 35 dB;

- T_{nFi} are the front end amplifier noise temperatures, evaluated from dedicated tests.

The insertion losses, noise temperatures and gains are estimated from dedicated ground measurements, while the physical temperatures, sky temperature, and the r parameter are quantities measurable in flight, it is thus apparent from the above expression that our ability to predict the transfer function and thermal susceptibility in flight depends fundamentally on our knowledge of $\frac{\partial G_F}{\partial T_{\text{phys}}^{\text{FEM}}}$ and $\frac{\partial T_{nF}}{\partial T_{\text{phys}}^{\text{FEM}}}$.

A requirement of our analysis is then to estimate these important parameters.

3 Thermal susceptibility test

During the flight model ground test campaign, the thermal susceptibility of front end modules to temperature fluctuations was measured both at the level of single RCAs and at the level of integrated instrument in the RAA cryogenic facility.

The RCA tests were performed with environmental and boundary conditions under a better control because of smaller dimensions involved and a more accurate monitoring was achieved due to dedicated temperature sensors in a smaller number of relevant interfaces; reference results are then taken from these.

In figure 2, a schematic view of a single RCA integrated in the test chamber [10] is shown.

The RAA thermal susceptibility tests have been performed in order to check consistency with the RCA results. Unfortunately, they were performed in non-ideal conditions so that a straight comparison with RCA tests is actually quite poor.

3.1 Test methods and procedures

The test philosphy and, accordingly, its procedure are very simple. The test was performed by changing the temperature of a single FEM (RCA test), or of the whole Focal Plane Unit (RAA test), and by measuring the radiometer output during the subsequent steady state period; the number of the steps was chosen in order to scan a temperature range of about 5K around the nominal value. Typical temperature curves and voltage output obtained during RCA tests are shown in figure 3.

In order to disentangle variations in the signal due to changes of FPU temperature from other sources of instability, the temperatures of all the main parts of the cryogenic chamber, in particular sky and reference loads, are monitored and their stability is controlled at the level of few mK.

3.2 Experimental setup

The RCA and RAA cryogenic chambers are described in [10] and [7], respectively.

The chamber thermal environment reproduces accurately the actual flight environment, with the exception of the sky and reference loads temperatures.
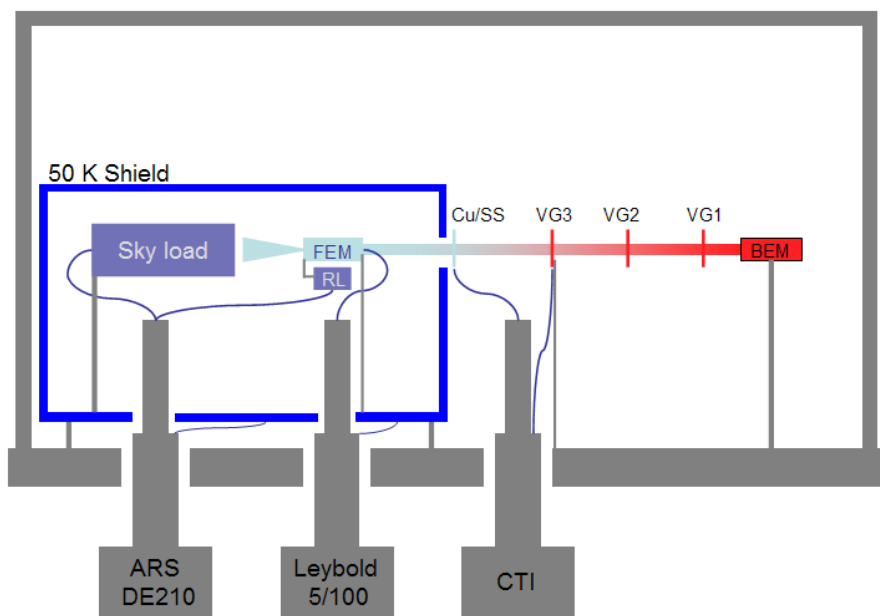
Figure 2. A schematic view of the 30 and 44 GHz RCA thermal setup integrated in the cryogenic chamber (from [10]). The feed horn receives the signal from the sky simulator in front of it; the signal is mixed in the FEM with the signal coming from the reference load and amplified. The long waveguides finally transmit the signal to the BEM detectors. In the thermal susceptibility tests, the temperature of the FEM is varied while reference and sky load temperatures are kept constant.
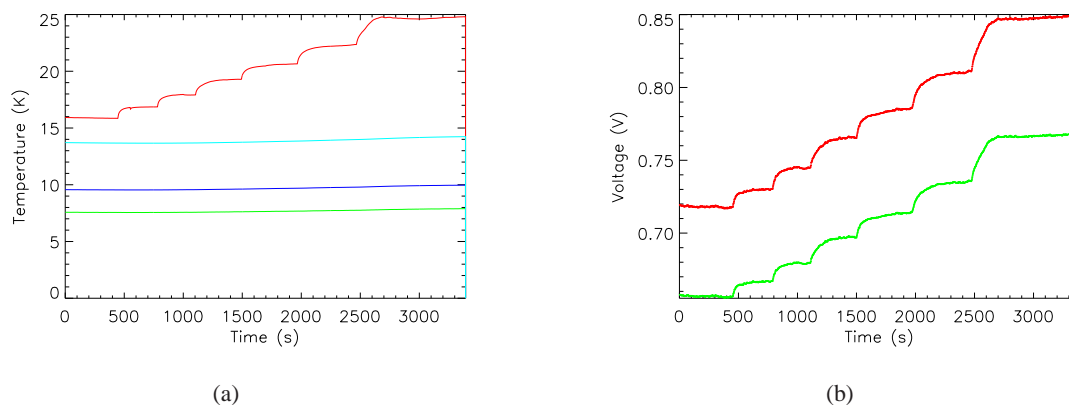

(a)

(b)

Figure 3. An example of THF test. Data are taken from RCA22 test, one of the 70 GHz radiometers. In (a) temperature data for FEM (red), ref (green), sky backplate (blue) and absorber (light blue) are shown: as evident here the FEM temperature has to change significantly, while reference and sky loads have to be kept at a temperature as stable as possible. Corresponding detector outputs are displayed in (b): sky is in red and ref in green.

However, the most important test feature is the temperature stability of the two loads, which are kept within an optimal level, so that the test results, obtained in an optimized and controlled environment, can be easily extrapolated to the flight conditions. This is also true for the test described

Figure 4. In the 30/44 GHz setup the heater and the sensor dedicated to the control of the FEM temperature are located on a flange directly screwed to the front end.
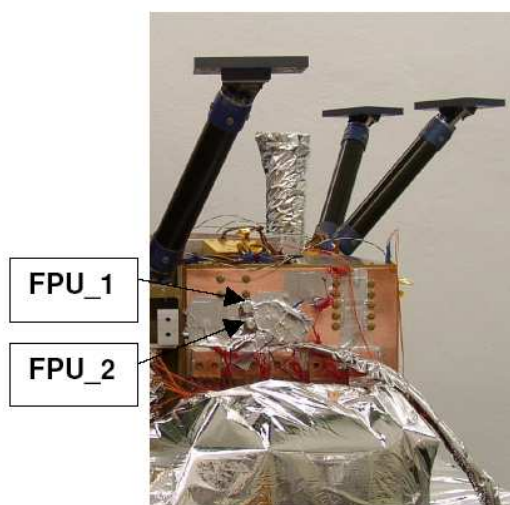

Figure 5. Main frame and FPU setup for the thermal vacuum tests. Nominal and redundant sensor dedicated to the control of the FPU temperature are shown, while heaters are fixed by Aluminum tape.

here.

The temperature control for the FEM thermal susceptibility tests (THF tests) is implemented through heaters, mounted on the interface between the front end and the flanges connected to the chamber reference cold end at 20 K, and temperature sensors, used to control the heaters and to monitor the FPU temperatures.

In the case of the RCA tests, a single FEM is connected to a cold finger with a copper flange where one heater and one sensor are mounted (figure 4).

At instrument level, the heater and corresponding sensor are mounted on a large copper flange, which mimics the sorption cooler cold end interface to the LFI main frame (figure 5). The corresponding temperature at the level of single FEMs is chosen from one of the sensors, whose detailed positions are shown in figure 6.
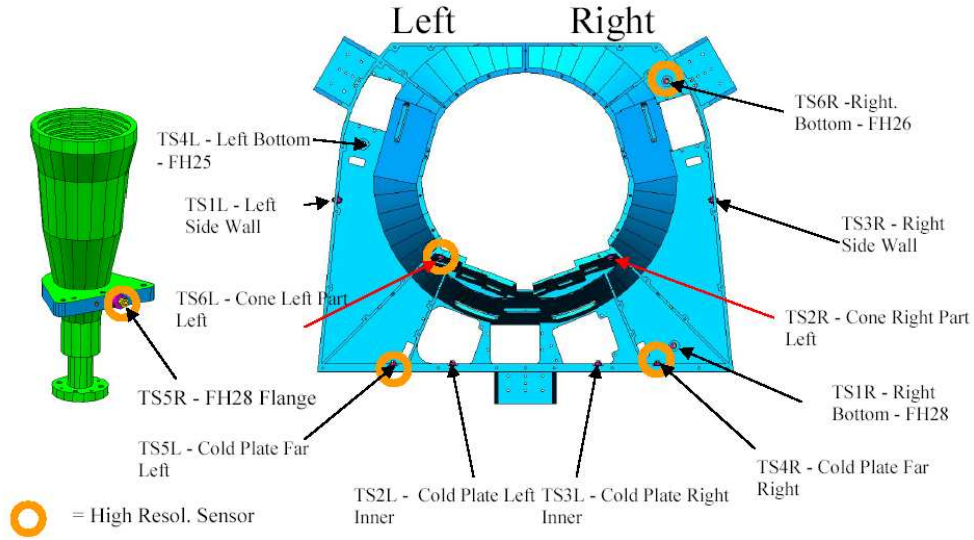
Figure 6. Sensors location in the LFI FPU and main frame. High sensitivity sensors are marked with circles.

3.3 Data analysis

For each value of the front-end temperature, $T_{\mathrm{phys}}^{\mathrm{FE}}$, we measured the receiver response (see figure 3), and then calculated the average receiver differential output, δT_{ant}, using the same value of the gain modulation factor, r, that was calculated in nominal front-end temperature conditions.

It is then possible to produce a plot of δT_{ant} vs. $\delta T_{\mathrm{phys}}^{\mathrm{FE}}$, where $\delta T_{\mathrm{phys}}^{\mathrm{FE}} = T_{\mathrm{phys}}^{\mathrm{FE}} - T_{\mathrm{phys-nominal}}^{\mathrm{FE}}$ (see figure 7).

From eq. (2.4), the transfer function is the slope of the curve obtained by linear fitting the points in the plot.

As explained above, the main unknown susceptibility parameters in eq. (2.5) are the amplifier noise temperature and gain variations with temperature.

In order to estimate them, their values is varied in the analytical expression of eq. (2.5), so to obtain a value consistent with the measured one. The predicted points and curve are in blue in figure 7.

The RaNA data analysis tool ([12]) for the RCA tests has a built-in THF module in order to automatically select useful data for this kind of test, calculate the fitted and measured values, and write a report of the test with table of results, best fit parameters and plots (figure 8).

These results are our best guesses for the intrinsic properties of the LFI amplifiers affected by the temperature fluctuations. The analytical values obtained assume a symmetric behaviour of the amplifiers corresponding to the two legs of the radiometer analyzed.

4 Results and discussion

The RCA calibration tests produced the most accurate results due to a dedicated test setup.

Actually, some problems during instrument level verification tests did not allowed a straight comparison between test results. They were due to radiometer settings (non optimal bias set during the first run) or to large thermal drifts (as occurred in the second run).
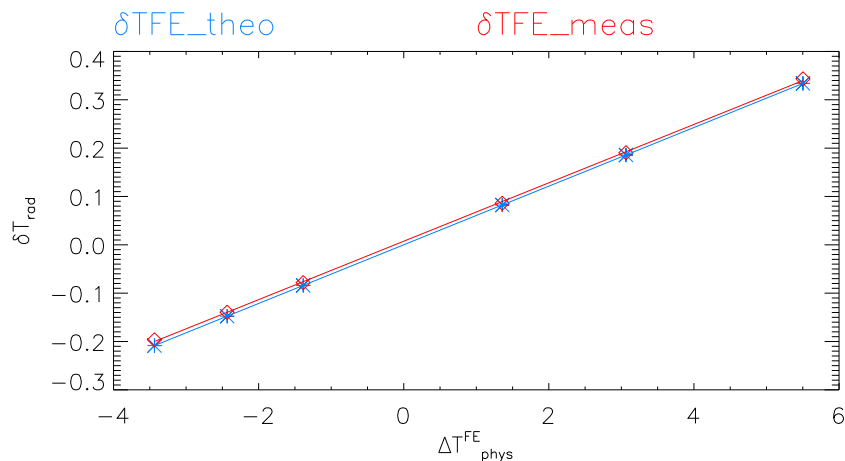
Figure 7. Radiometer thermal susceptibility analysis. Data are taken from the RCA22 test again. Experimental measured (red) and Analytical prediction (blue) are plotted. Measurement errors are within the symbol sizes.
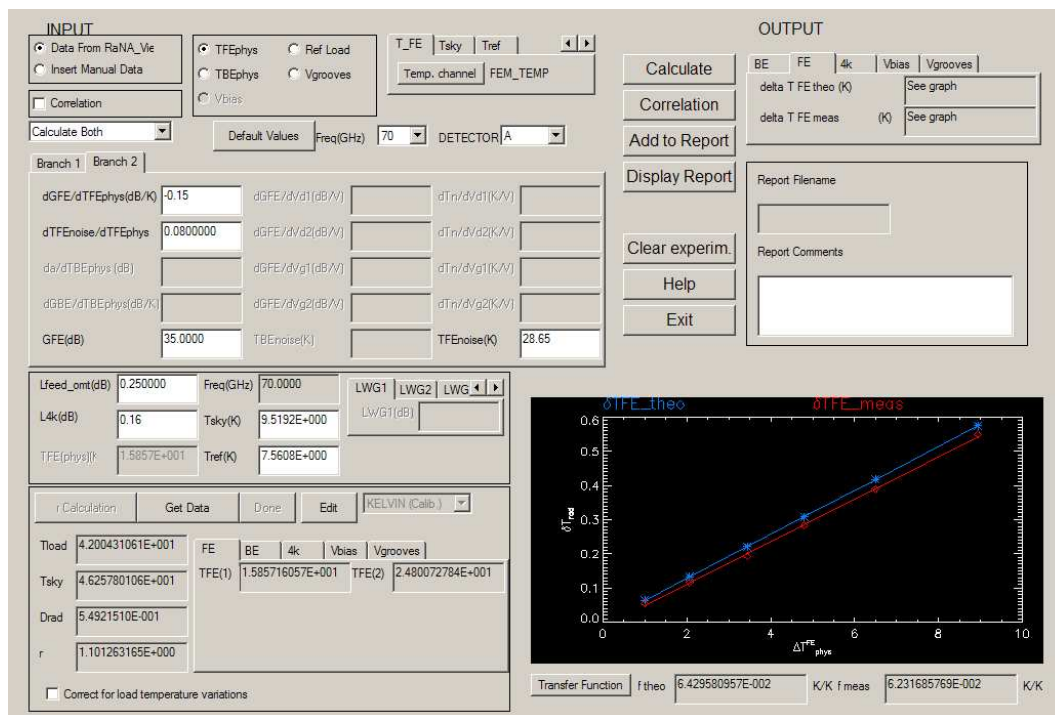

Figure 8. Layout of the RaNA_Susc module of the LIFE data analysis tool. It allows to get automatically voltage and temperature data useful for the estimation of the thermal susceptibility, calculate the transfer function and compare it to the analytical one, using default or user-defined parameters.

Moreover, not all the radiometer amplifiers are closely monitored by thermometers (figure 6) and the choice of the best temperature sensor to associate to the FEM under test was not always straightforward, and finally the most accurate sensors have a limited range of calibration. Since the temperatures reached during the instrument level thermal susceptibility test were outside this calibration range, a number of thermometers were therefore not used for the data analysis (see
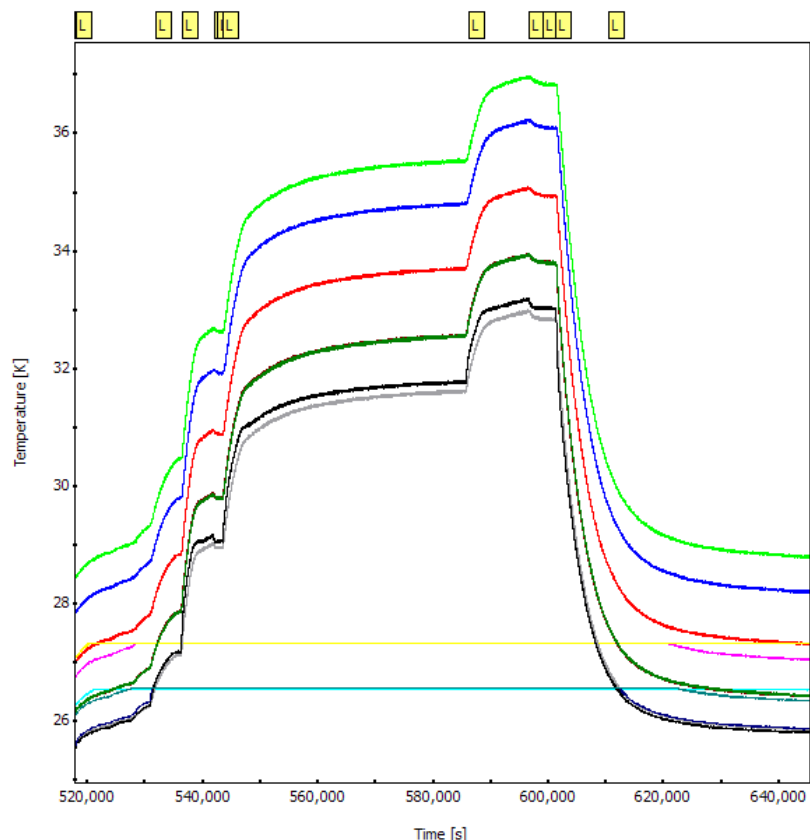
Figure 9. FPU sensors temperature curve. The five high resolution sensors are out of range for most of the steps. This is evident from the straight horizontal lines in the middle of the plot: when sensors go higher than their upper calibration limit their output is fixed to that value until their temperature goes back in the calibration curve range.

figure 9).

Figure 10 shows a comparison between the predicted transfer functions and the ones measured during RAA tests. The predicted results come from the analytical formula 2.5, using RAA measured environmental data and radiometer intrinsic properties ($\frac{\partial G_F}{\partial T_{\mathrm{phys}}^{\mathrm{FEM}}}$ and $\frac{\partial T_{nF}}{\partial T_{\mathrm{phys}}^{\mathrm{FEM}}}$) estimated from RCA tests. This is reported only for those radiometer channels correctly biased during the RAA test performed in more stable conditions.

Considering the limitations affecting the measurement the agreement is good for most of the channels.

Detailed results from the RCA flight model test campaign are reported in the appendix.

All values are contained in the range $(1 \div 100)$ $\frac{mK}{K}$, with higher values (50 to 120 $\frac{mK}{K}$) for the 70 GHz channels (except RCA 21 Side radiometer), so that, depending on the radiometer, the physical temperature fluctuations of the front end module are reduced by a factor of 10 to 1000. This effect is actually flat in the frequency space and it is applied at the end of the path of thermal instabilities already filtered by the thermo-mechanical structure of the LFI focal plane (detailed in [11]).

Taking into account the source of temperature fluctuations, reduced by means of the active control at the order of 100 mK peak-to-peak and considering all the reduction factors, we can estimate to less than 1 mK peak-to-peak in the radiometer output data stream. A further reduction
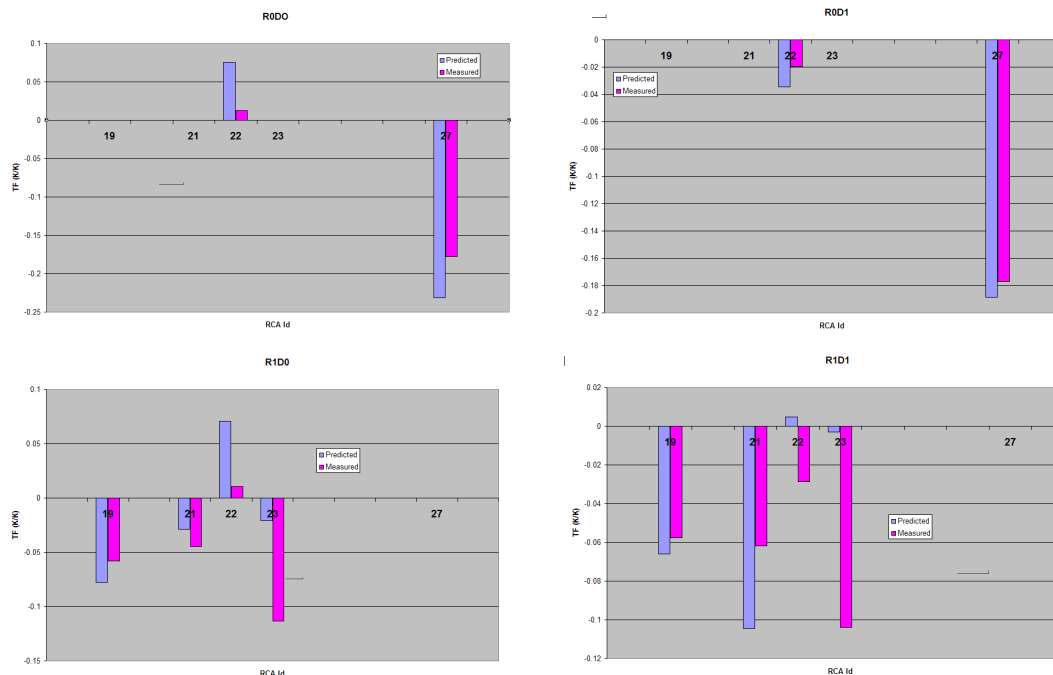
Figure 10. Comparison between predicted and measured transfer functions during instrument level tests for the channels properly biased. Radiometers Main and Side are labelled as R0 and R1, while detectors outputs as D0 and D1, for each radiometer leg. The predicted transfer functions are obtained from the analytical expression using radiometric parameters found in RCA tests and environmental parameters measured in the RAA test itself.

of the effect at the different frequency components of the order of about 200 - 500 times occurs in the map making and destriping procedures, as estimated in [4].

The final result is that temperature fluctuations generated by the 20 K sorption cooler and propagated through the LFI focal plane are kept at the level of the required error budget.

A by-product of our analysis is the information about the temperature dependance of amplifiers noise temperature and gain, which are shown in the appendix tables. The range of gain susceptibility is -0.01 – -0.08 $\frac{dB}{K}$ with some major exception for the RCA 22 and 28. The temperature variations of amplifiers noise temperatures ranges between 0.1 and 0.8 $\frac{K}{K}$.

Due to dependance of the transfer functions on input temperatures and *r* parameter (eq. (2.5)), these are important sources of information allowing the estimation of the impact of in-flight temperature fluctuations on the measured signal and on CMB recovery.

A Radiometer output equation

The output of a LFI Back End detector can be analytically expressed as:

$$V_{\text{out}} = a \cdot k \cdot \beta \cdot G_B \left\{ \left[(G_{F1} + G_{F2}) \cdot \left(\frac{G_{F1}T_{nF1} + G_{F2}T_{nF2}}{2L_{WG}} \right) + \left(1 - \frac{1}{L_{WG}} \right) \cdot T_{WG}^{\text{eff}} + T_{nB} \right] \cdot (1 - r) \right.$$
$$\left. + \frac{\sqrt{G_{F1}G_{F2}}}{L_{WG}} \left(T_{\text{sky}} - T_{\text{ref}} \right) \cdot (1 + r) \right\} \quad \text{(A.1)}$$

where:

- a is the square law detector constant

- β is the radiometer bandwidth

- k is the Boltzmann constant

- L_i are the RF losses of the different stages of the radiometer chain

- G_i and T_{ni} are the FEM and BEM amplifiers gains and noise temperatures

- T_{sky} and T_{ref} are the equivalent sky and ref antenna temperatures exiting the Front End.

- T_{WG}^{eff} is the effective waveguide temperature as integrated through its route.

More details can be found in [1, 8]

B Thermal susceptibility detailed results

In this section a summary of the transfer function measurements is given. Temperature dependance of LNAs gain and noise temperature are also estimated from the comparison between the measured and the analytically estimated transfer functions, in the hypothesis of perfectly symmetrical coupled amplifiers.

Table 1. RCA18 thermal susceptibility results.

Ch	S-11	S-10	M-00	M-01
$\frac{\partial G}{\partial T}$ (dB/K)	-0.05 ± 0.005	-0.05 ± 0.005	-0.05 ± 0.005	-0.05 ± 0.005
$\frac{\partial Tn}{\partial T}$ (K/K)	0.42 ± 0.02	0.38 ± 0.02	0.47 ± 0.02	0.49 ± 0.02
f_{meas} (mK/K)	-77 ± 3	-68 ± 4	-85 ± 5	-91 ± 4

Table 2. RCA19 thermal susceptibility results.

Ch	S-11	S-10	M-00	M-01
$\frac{\partial G}{\partial T}$ (dB/K)	-0.03 ± 0.005	-0.023 ± 0.005	-0.05 ± 0.005	-0.035 ± 0.005
$\frac{\partial Tn}{\partial T}$ (K/K)	0.37 ± 0.02	0.4 ± 0.02	0.36 ± 0.02	0.33 ± 0.02
f_{meas} (mK/K)	-111 ± 10	-120 ± 9	-94 ± 7	-9 ± 8

Table 3. RCA20 thermal susceptibility results.

Ch	S-11	S-10	M-00	M-01
$\frac{\partial G}{\partial T}$ (dB/K)	-0.039 ± 0.005	-0.03 ± 0.005	-0.049 ± 0.005	-0.0408 ± 0.005
$\frac{\partial Tn}{\partial T}$ (K/K)	0.25 ± 0.02	0.3 ± 0.02	0.25 ± 0.02	0.23 ± 0.02
f_{meas} (mK/K)	-58 ± 7	-59 ± 7	-66 ± 8	-57 ± 8

Table 4. RCA21 thermal susceptibility results.

Ch	S-11	S-10	M-00	M-01
$\frac{\partial G}{\partial T}$ (dB/K)	-0.2 ± 0.05	-0.07 ± 0.005	-0.07 ± 0.005	-0.07 ± 0.005
$\frac{\partial Tn}{\partial T}$ (K/K)	0.3 ± 0.02	0.18 ± 0.02	0.15 ± 0.02	0.15 ± 0.02
f_{meas} (mK/K)	-9.3 ± 0.8	-7.7 ± 0.9	-30.1 ± 0.9	-18 ± 1

Table 5. RCA22 thermal susceptibility results.

Ch	S-11	S-10	M-00	M-01
$\frac{\partial G}{\partial T}$ (dB/K)	-0.13 ± 0.005	-0.175 ± 0.005	-0.213 ± 0.005	-0.15 ± 0.005
$\frac{\partial Tn}{\partial T}$ (K/K)	0.1 ± 0.02	0.1 ± 0.02	0.1 ± 0.02	0.1 ± 0.02
f_{meas} (mK/K)	60.4 ± 0.4	56.9 ± 0.8	56.7 ± 0.6	52.1 ± 0.7

Table 6. RCA23 thermal susceptibility results.

Ch	S-11	S-10	M-00	M-01
$\frac{\partial G}{\partial T}$ (dB/K)	-0.05 ± 0.005	-0.05 ± 0.005	-0.03 ± 0.005	-0.05 ± 0.005
$\frac{\partial Tn}{\partial T}$ (K/K)	0.16 ± 0.02	0.17 ± 0.02	0.1 ± 0.02	0.16 ± 0.02
f_{meas} (mK/K)	-39 ± 3	-41 ± 4	-21 ± 2	-44 ± 3

Table 7. RCA24 thermal susceptibility results.

Ch	M-00	M-01	S-11	S-10
$\frac{\partial G}{\partial T}$ (dB/K)	-0.08 ± 0.005	-0.063 ± 0.001	-0.08 ± 0.005	-0.081 ± 0.001
$\frac{\partial Tn}{\partial T}$ (K/K)	0.4 ± 0.02	0.41 ± 0.02	0.43 ± 0.02	0.1 ± 0.02
f_{meas} (mK/K)	-12.1 ± 0.1	-6.10 ± 0.08	-9.6 ± 0.5	-20.3 ± 0.7

Table 8. RCA25 thermal susceptibility results.

Ch	S-11	S-10	M-00	M-01
$\frac{\partial G}{\partial T}$ (dB/K)	-0.045 ± 0.005	-0.042 ± 0.005	-0.022 ± 0.005	-0.02 ± 0.005
$\frac{\partial Tn}{\partial T}$ (K/K)	0.08 ± 0.02	0.25 ± 0.02	0.12 ± 0.02	0.1 ± 0.02
f_{meas} (mK/K)	-22.1 ± 0.7	-29 ± 2	-15.1 ± 0.9	-13 ± 0.5

Table 9. RCA26 thermal susceptibility results.

Ch	M-00	M-01	S-10	S-11
$\frac{\partial G}{\partial T}$ (dB/K)	-0.01 ± 0.005	-0.026 ± 0.005	-0.01 ± 0.005	-0.01 ± 0.005
$\frac{\partial Tn}{\partial T}$ (K/K)	0.7 ± 0.02	0.7 ± 0.02	0.47 ± 0.02	0.5 ± 0.02
f_{meas} (mK/K)	-66 ± 2	-64 ± 2	-68 ± 1	-65.6 ± 0.9

Table 10. RCA27 thermal susceptibility results.

Ch	M-00	M-01	S-11	S-10
$\frac{\partial G}{\partial T}$ (dB/K)	-0.055 ± 0.005	-0.05 ± 0.005	-0.01 ± 0.005	-0.04 ± 0.005
$\frac{\partial Tn}{\partial T}$ (K/K)	0.81 ± 0.02	0.45 ± 0.02	0.34 ± 0.02	0.58 ± 0.02
f_{meas} (mK/K)	-16.8 ± 0.5	-10.5 ± 0.5	-31 ± 3	-36 ± 2

Table 11. RCA28 thermal susceptibility results.

Ch	S-10	S-11	M-00	M-01
$\frac{\partial G}{\partial T}$ (dB/K)	-0.13 ± 0.005	-0.14 ± 0.005	-0.03 ± 0.005	-0.067 ± 0.005
$\frac{\partial Tn}{\partial T}$ (K/K)	0.33 ± 0.02	0.1 ± 0.02	0.15 ± 0.02	0.15 ± 0.02
f_{meas} (mK/K)	-11 ± 2	-19 ± 2	-2.7 ± 0.7	5.2 ± 0.8

References

[1] M. Bersanelli et al., *Planck pre-launch status: Design and description of the Low Frequency Instrument*, accepted by *Astron. Astrophys.* (2009).

[2] J.M. Lamarre et al., *Planck pre-launch status: the HFI instrument, from specification to actual performance*, submitted to *Astron. Astrophys.* (2009).

[3] N. Mandolesi et al., *Planck pre-launch status: the Planck-LFI program*, accepted by *Astron. Astrophys.* (2009).

[4] Mennella, A. , Bersanelli, M., Burigana, C., et al., 2001, A&A, 384, 736 *Planck: systematic effects induced by periodic fluctuations of arbitrary shape*, *Astron. Astrophys.* **384** (2009) 736.

[5] A. Mennella et al., *Planck pre-launch status: Low Frequency Instrument calibration and scientific performance*, accepted by *Astron. Astrophys.* (2009).

[6] G. Morgante et al., *Cryogenic characterization of the Planck sorption cooler system flight model*, 2009 *JINST* **4** T12016.

[7] G. Morgante et al., *The cryogenic setup for ground testing of the Planck-LFI instrument*, in preparation (2009).

[8] M. Seiffert et al., *1/f noise and other systematic effects in the Planck-LFI radiometers*, *Astron. Astrophys.* **391** (2002) 1185.

[9] J. Tauber et al., *Planck pre-launch status: the Planck mission*, accepted by *Astron. Astrophys.* (2009).

[10] L. Terenzi et al., *Cryogenic environment and performance for testing the Planck radiometers*, 2009 *JINST* **4** T12015.

[11] M. Tomasi et al., *Dynamic validation of the Planck-LFI thermal model*, in preparation (2009).

[12] M. Tomasi et al., *Off-line radiometric analysis of Planck-LFI data*, 2009 *JINST* **4** T12020.

[13] L. Valenziano et al., *Planck-LFI: design and performance of the 4 Kelvin Reference Load Unit*, 2009 *JINST* **4** T12006.

[14] F. Villa et al., *Planck pre-launch status: calibration of LFI flight model radiometers*, submitted to *Astron. Astrophys.* (2009).